PCCP

PAPER

View Article Online
View Journal | View Issue

Cite this: *Phys. Chem. Chem. Phys.*, 2015, **17**, 12207

Dielectric and Raman investigations of structural phase transitions in $(C_2H_5NH_3)_2CdCl_4$†

Ruchika Yadav,*[a] Diptikanta Swain,[b] Partha P. Kundu,[bc] Harikrishnan S. Nair,[de] Chandrabhas Narayana[b] and Suja Elizabeth[a]

Received 12th February 2015,
Accepted 2nd April 2015

DOI: 10.1039/c5cp00906e

www.rsc.org/pccp

Temperature-dependent Raman and dielectric measurements have been carried out on $(C_2H_5NH_3)_2CdCl_4$ single crystals. Raman studies reveal the presence of two structural phase transitions below room temperature at 216 K and 114 K. The phase transitions are marked by anomalies in temperature dependence of wave-number and full width half maximum (FWHM) of several vibrational modes. The transitions are also accompanied by anomalies in dielectric measurements. Raman and dielectric data indicate that the transition at 216 K is order–disorder in nature and is driven by re-orientation of organic ions, while the transition at 114 K is due to coupling between the $CdCl_6$ octahedron and the organic chain. Further high temperature dielectric measurements reveal the presence of one more structural phase transition around 473 K across which dispersion in dielectric parameters is observed. The activation energies and relaxation time obtained for high temperature dielectric phases are characteristic of combined reorientation motions of alkyl ammonium cations.

1 Introduction

Hybrid organic–inorganic perovskite materials are few of the most extensively studied crystalline hybrid compounds, by virtue of their multifunctional behaviour and potential applications.[1–7] They consist of a wide range of inorganic anion chains (an extended network of corner-sharing metal oxide or halide complexes), alternating with a large variety of organic cations as building blocks. The organic component of the hybrid complex provides several useful properties such as structural flexibility, optical properties, *etc.*, while the inorganic part is responsible for mechanical and thermal stability, interesting magnetic and dielectric transitions, *etc.*[4,8–10] We can combine the useful properties of organic and inorganic components at the single molecular level to tailor new multifunctional materials. Few such examples are $[(CH_3)_2NH_2]Mn(HCOO)_3$[11,12] and $[NH_4]Mn(HCOO)_3$,[13] metal organic frameworks with perovskite structure. Both materials show transitions from a disordered state to an ordered state at low temperature as a result of hydrogen bonding between organic and inorganic components. $[(CH_3)_2NH_2]Mn(HCOO)_3$[11] undergoes paraelectric to antiferroelectric transition at 185 K, while $[NH_4]Mn(HCOO)_3$[13] transforms to the ferroelectric phase below 250 K, both being accompanied by structural transition. The compounds show weak ferromagnetism at temperatures below 10 K. This demonstrates that the organic and inorganic parts can be chosen and optimized to allow compositions with desirable multifunctional characteristics.

In this respect, crystals of metal ion complexes with organic molecules are worth revisiting. Of particular interest were crystals of alkyl ammonium metal halides $(C_nH_{2n+1}NH_3)_2MCl_4$ (M = Mn, Cu, Cd, Fe). These belong to a family of ABX_3 perovskite consisting of nearly isolated layers of corner-sharing MCl_6 octahedrons sandwiched by alkyl-ammonium cations $(C_nH_{2n+1}NH_3)^+$ abbreviated as MA (methyl-ammonium) for n = 1 and EA (ethyl-ammonium) for n = 2.[14–16] The ammonium groups of the alkyl ammonium cations are present in the cavities between the M–Cl octahedron, and forms N–H$\cdots$Cl hydrogen bonds with them. The adjacent layers are stacked upon each other through van der Waals forces between the terminal methyl groups. Additionally coulomb interactions are also present between transition metal ions (negatively charged octahedron) and organic cations. The interaction between two layers is much weaker compared to intra-layer interactions.

These compounds usually self-assemble at ambient temperature from solutions and are stable up to 200 °C. They display a variety of physical properties depending on the transition metal cation.

[a] *Department of Physics, Indian Institute of Science, Bangalore – 560012, India. E-mail: ruchika@physics.iisc.ernet.in*
[b] *Chemistry and Physics of Materials Unit, Jawaharlal Nehru Centre for Advanced Scientific Research, Jakkur, P.O., Bangalore 560064, India*
[c] *Department of Physics, M.S. Ramaiah University of Applied Sciences, Bangalore – 560058, India*
[d] *Highly Correlated Matter Research Group, Physics Department, University of Johannesburg, P.O. Box 524, Auckland Park 2006, South Africa*
[e] *JCNS 2/Peter Grünberg Institute 4, Forschungszentrum Jülich, 52425 Jülich, Germany*

† Electronic supplementary information (ESI) available. See DOI: 10.1039/c5cp00906e

For Cu, the system exhibits multiferroic behaviour where ferroelectric ordering is observed below 250 K and magnetic spins align antiferromagnetically below 8 K.[17] A non-magnetic semiconducting nature is observed for Pb while the Cd and Zn analogues show insulating behaviour.[18] The crystal structure varies with temperature and pressure.[19–21] All compounds of this series show orthorhombic structure at room temperature and undergo a series of structural changes due to different arrangements of alkyl ammonium chains. The choice of the hydrogen bonding scheme is important in determining the orientation of organic molecule, thereby influencing the structural phase transition.[22] Cd and Mn analogues, represent the pseudo tetragonal lattice, and the system transforms to tetragonal symmetry by a small shift in the mean positions of atoms. At higher temperature, the compounds display orthorhombic to tetragonal structural transition at 394 K for M = Mn^{2+} and 484 K for M = Cd^{2+} respectively.[21] Two more structural transitions are observed at low temperatures (at 114 K and 216 K for M = Cd).[21,23] In the present investigation, we have analysed the mechanism of phase transitions in $(C_2H_5NH_3)_2CdCl_4$ using temperature dependent dielectric studies and Raman spectroscopy. Dielectric measurements provide insight into the transport mechanism across the transition, at the same time Raman spectroscopy captures the dynamics and local structural changes with temperature.

2 Experimental

Single crystals of $(C_2H_5NH_3)_2CdCl_4$ (EA–$CdCl_4$) were grown by slow evaporation from an aqueous solution containing stoichiometric amounts of precursors, as described elsewhere.[24] The quality of the crystals used for experiments was checked under a polarizing microscope. For dielectric measurements silver electrodes were deposited on oriented samples. All temperature and frequency dependent dielectric measurements were carried out in the temperature range 50 to 300 K, in a Closed Cycle Refrigerator using an Agilent 4294 A Precision Impedance Analyser. The temperature evolution of Raman Spectra of $(C_2H_5NH_3)_2CdCl_4$ was recorded in the 180° backscattering geometry using 532 nm excitation from a diode pumped frequency doubled Nd:YAG solid state laser (model GDLM-5015 L, Photop Suwtech Inc., China) and a custom-built Raman spectrometer equipped with a spex triax 550 monochromator and a liquid nitrogen CCD (spectrum one with CCD 3000 controller, ISA Jobin Yovn).[25] The laser power on the sample was about 6 mW, and a typical spectral acquisition time of 4 min was used with a spectral resolution of 2 cm^{-1}. The temperature was controlled with an accuracy of (±0.1) K with the help of a temperature controller equipped with a cooling stage (Linkam THMS 600). The spectral profile was fitted using a Lorentzian function with the appropriate background.

All density functional theory (DFT) calculations were performed using the Gaussian 09 program[26] and geometrical optimization was carried out using the hybrid exchange–correlation functional Becke3-Lee-Yang-Parr (B3LYP).[27,28] Basis sets of C, H, N and Cl atoms were chosen 6-31G(d) and the valence and inner shell electrons of Cd atoms were described by basis set LANL2DZ and the corresponding relativistic effective core potential respectively.[29] In order to mimic the solid environment 12 organic components and 2 $CdCl_2$ units were chosen as shown in Fig. 1. The organic units at the corners were frozen in order to prevent the structure from collapse in the gas phase since the charges in each fragments are opposite in polarity. The harmonic Raman frequencies were computed on the optimized structures using the same level. Since the theoretical approach and basis set is incomplete, and an-harmonicity is neglected, the experimental data and theoretically calculated values were matched with a scaling factor of 0.961[30] for frequencies above 1000 cm^{-1}.

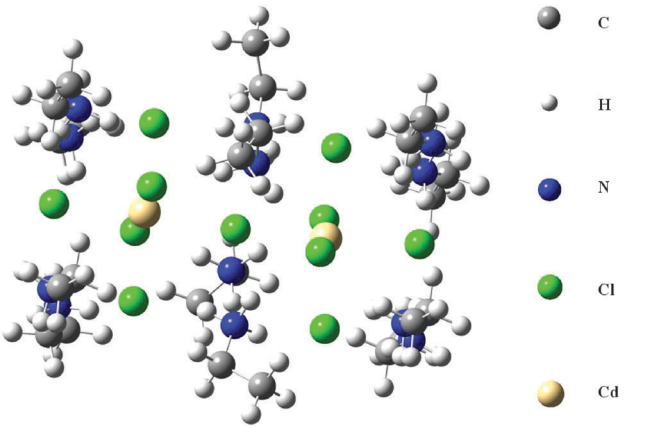

Fig. 1 Structure of $(C_2H_5NH_3)_2CdCl_4$ used for calculating Raman modes using the Gaussian software.

3 Results and discussions

3.1 Dielectric measurements

Presence of organic molecules with dipoles and the two-dimensional structure of EA–XCl_4 (X = Cu, Cd, Mn, Fe) lead to interesting behaviour in these compounds. The dielectric behaviour in the temperature ranges (10–300) K and (300–500) K, at frequencies between 100 Hz and 1 MHz are probed in EA–$CdCl_4$. Three structural transitions are observed around 475 K (T_{c1}), 214 K (T_{c2}) and 116 K (T_{c3}), in the heating cycle. The dielectric response with transition (T_{c2}) has been previously reported.[31] For a single crystalline c-plate, temperature dependent dielectric response in both heating and cooling runs for a temperature range 10 K to 300 K is shown in Fig. 2.

Dielectric values decrease upon cooling and anomalies are seen at temperatures 212 K and 95 K both of which correspond to structural transitions (transition temperatures estimated by the 1st order derivative of the dielectric constant). A clear hysteresis is clearly observed in heating and cooling cycles at both transitions which indicate that the transition is first order in nature. The hysteresis width at T_{c3} transition is higher than that observed at T_{c2}, which is likely due to the broad temperature region over which the transition at T_{c3} occurs. The magnitude of the dielectric constant observed parallel to the plane of the crystal are much larger as compared to the values observed

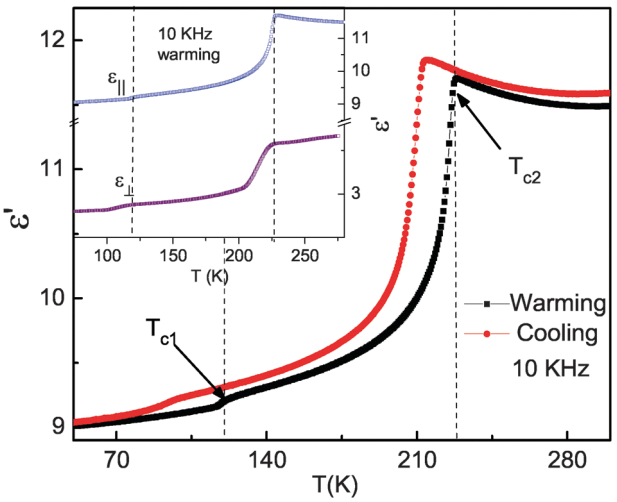

Fig. 2 Temperature evolution of dielectric constants at 10 kHz frequency in both cooling and heating cycles. Inset shows temperature evolution of dielectric constants, both parallel and perpendicular to the crystal plate.

for in the plane perpendicular to the crystal as shown in the inset of Fig. 2 (data collected during the heating cycle). Though the transition resembles an antiferroelectric ordering and there is presence of a low temperature anti-polar monoclinic phase, no antiferrolectric hysteresis loop is seen in PE loop measurements. The temperature at which the dielectric anomaly is observed does not shift with frequency but the magnitude of dielectric constant falls sharply as the frequency increases. Temperature variation of dielectric parameters ε_1 (dielectric constant) and ε_2 (dielectric loss) in the temperature range (320–500) K is presented in Fig. 3 and inset. The anomaly observed around 475 K (T_{c1}) is attributed to a structural phase transition. The high temperature transition in this compound has not been explored in detail so far, although similar transitions have been documented for EA–$MnCl_4$ and $(CH_3NH_3)_2FeCl_4$[32,33] and assigned to the structural transition from the tetragonal ($P4/mmm$) to orthorhombic phase. In many

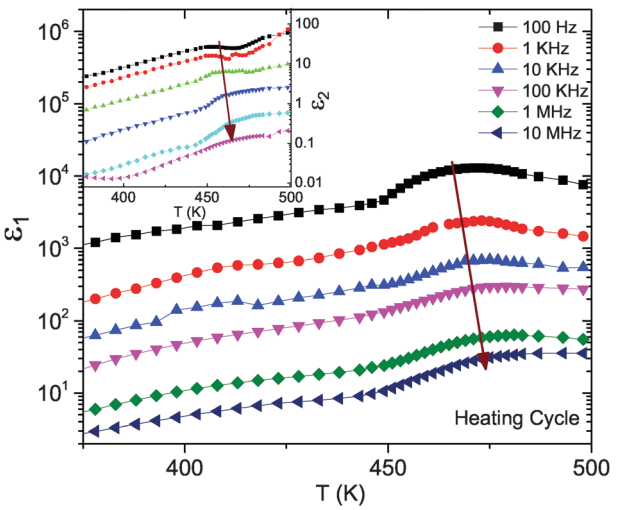

Fig. 3 Temperature evolution of dielectric constants in the temperature range (350–500) K for different frequencies.

materials there is no dispersion observed in the dielectric permittivity with frequency, across structural phase transition.[34] However in many hybrid organic–inorganic compounds, dielectric relaxation/dispersion is observed across the transition due to reorientation of organic molecules.[32,35,36] Such a relaxation process is characteristic of compounds with alkyl-ammonium ions.[37] For the studied compound a small dispersion is observed across the structural transition as shown in Fig. 3, which arises from the combined motion of $(C_2H_5NH_3)^+$ cations.

To explore the relaxation process in EA–$CdCl_4$, we performed dielectric measurements in the range 100 Hz to 1 MHz at temperatures in the vicinity of the transition. The shape of curves fitted for the imaginary part of the dielectric constant (ε_2) as shown in Fig. 7 implies the existence of relaxation time distribution. The relaxation time distribution is then determined using Cole–Cole diagrams to elucidate the mechanism of relaxation.

$$\varepsilon^* = \varepsilon_1 + i\varepsilon_2 \quad (1)$$

$$= \varepsilon_\infty + (\varepsilon_0 - \varepsilon_\infty)/[1 + (i\omega\tau)^{1-\alpha}] \quad (2)$$

where ε_0 and ε_∞ are static (low frequency) and high frequency dielectric constants, ω is angular frequency and τ is mean relaxation time. α is a parameter representing the distribution of relaxation times ($\alpha = 0$ for ideal Debye relaxation). The observed values of α were in the range 0.45 to 0.53 showing a considerable change from ideal Debye like behavior. Eqn (1) is separated into real and imaginary parts as below.

$$\varepsilon_1 = \varepsilon_\infty + ((\varepsilon_0 - \varepsilon_\infty)/2)[1 - \sinh \beta z/((\cosh \beta z + \cos \beta\pi/2))] \quad (3)$$

and

$$\varepsilon_2 = ((\varepsilon_0 - \varepsilon_\infty)/2)[\sinh \beta z/(\cosh \beta z + \cos \beta\pi/2)] \quad (4)$$

where z is $\ln(\omega\tau)$ and β is $(1 - \alpha)$. The frequency dependence of $\varepsilon_2(T)$ is shown in Fig. 4 for a few select temperatures. For an inhomogeneous insulator, dielectric spectra have contributions from electrical conductivity. The above approximation allows us to account for the contribution of electrical conductivity separately. The detailed analysis of ac conductivity shows an exponential increase with temperature which is characteristic of the hopping mechanism. An anomaly is observed near the transition temperature as shown in Fig. 5(a).

The inset in Fig. 5(a) ($\ln(\sigma)$ *vs.* $1/T$) shows 2 linear segments and from the slope of these segments, we estimated the activation energy for both phases. The values obtained for E_a are in the range 0.9 to 0.5 eV which are commensurate with the energy values for weak hydrogen bonds. This result confirms the proton character of the conductivity.[38] Relaxation times are estimated by fitting the frequency dependent ε_2 at different temperatures, using eqn (3). The values of relaxation time are observed in the range 10^{-3}–10^{-6} s, characteristic of combined reorientation of ethyl-ammonium cations.[39] Similar values are observed for the relaxation in EA–$CuCl_4$.[32] The temperature dependence of the corresponding relaxation time is shown in Fig. 5(b), which represents a linear behaviour in the logarithmic

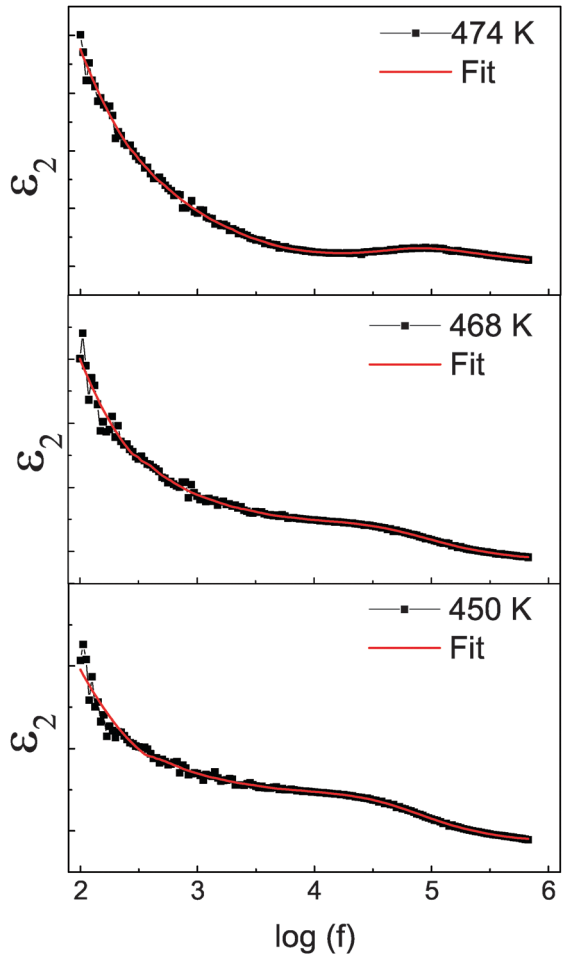

Fig. 4 Frequency dependence of the imaginary part of the dielectric constant at various temperatures.

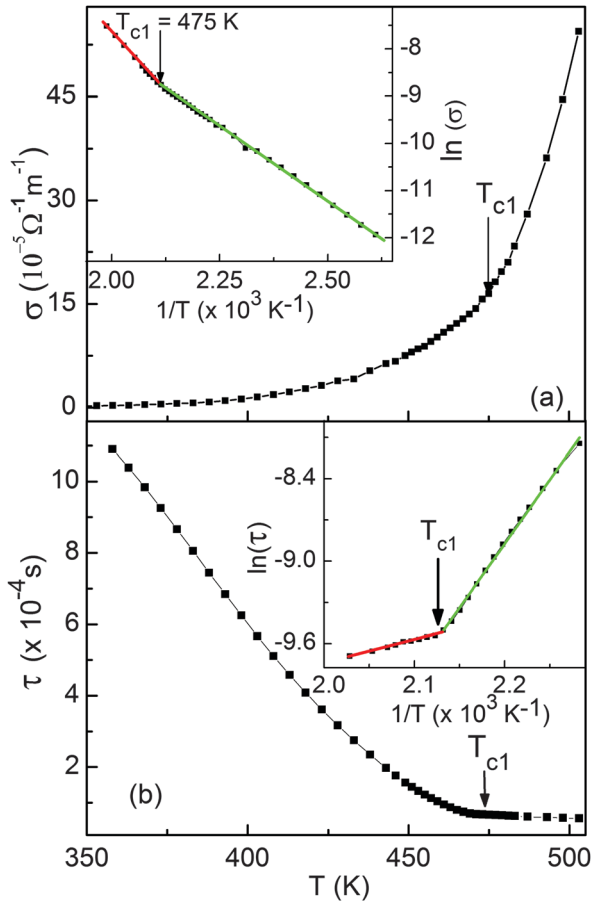

Fig. 5 (a) Variation of ac conductivity with temperature. Inset shows ln(σ(1/T)). (b) Variation of relaxation time with temperature. Inset shows ln(τ(1/T)).

scale (shown in the inset of Fig. 5(b)). The observed decrease in relaxation time with an increase in temperature is related to the decrease in hydrogen bond strength.

The activation energy (E_r) for the relaxor behaviour can be calculated using the Arrhenius equation.

$$\tau = \tau_0 \exp(E_r/kT) \quad (5)$$

The value of E_r obtained below the transition temperature is 0.715 eV, which is higher than the E_a value in the same region. The high temperature value of E_r is 0.124 eV which is small compared to E_a value in the same region. We have used impedance spectroscopy to study the multiple relaxations where different types of dielectric relaxations can be de-convoluted using an RC element model. For the ideal single relaxation Z'–Z'', the plot assumes the shape of a semicircle but considerable deviations are observed for real systems. In order to account for such non-ideal behaviour, the ideal capacitor is replaced with a constant phase element (CPE), with impedance defined as,

$$Z_{CPE}^{*} = 1/C_{CPE}(i\omega)^n \quad (6)$$

The impedance of the sample is measured at several temperatures and Z'–Z'' is plotted as shown in Fig. 5. The data are fitted using 2 R-CPE units corresponding to contributions from the bulk sample and the sample–electrode. The fitted curve for data corresponding to 450 K is shown in Fig. 6 along with the equivalent circuit used for fitting. The fit parameters are $R_1 = 45439 \pm 1.281\%$,

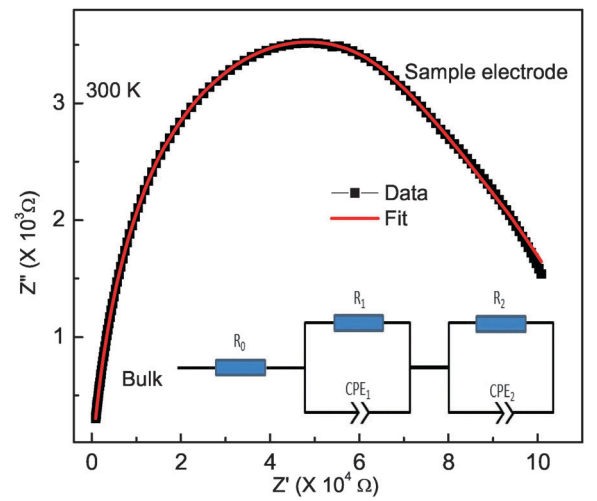

Fig. 6 Experimental Z'–Z'' plot with a fit, for the observed data at 300 K. Inset shows the equivalent circuit used to the model the complex plane of impedance.

R_2 = 66751 ± 0.361%, C_1 = 2.414 nF ± 1.365%, n_1 = 0.74 ± 0.142%, C_2 = 0.499 pF ± 0.820% and n_2 = 0.884 ± 0.068%. The high frequency response corresponds to the bulk contribution, while the low frequency response is related to the sample–electrode interface.

It is known that the alkyl-ammonium cation complexes are disordered at the highest temperature.[15] The NH_3 groups of organic cations occupy cavities in the metal halide octahedron and are linked to the metal halide complex by hydrogen bonding. At the highest temperature, the organic cations possess four equivalent states and they flip between these states. As the temperature decreases, the organic cation motion freezes stepwise from four to two and two to one at the corresponding transition temperatures (T_{c1} and T_{c2}). The low temperature monoclinic phase (at T_{c3}) is realized by non-linear coupling between the organic cation and the lattice. These results fairly co-relate with the lowering and dispersion in dielectric data obtained in the present study.

3.2 Raman spectroscopy

The vibrational spectra of the alkyl ammonium metal halide category of hybrid compounds can be divided into 2 regions. The region below 300 cm^{-1} describes external modes of the crystal including vibrations of the metal–halide octahedron, while the region above 300 cm^{-1} describes the internal vibrations of organic cations. Although Raman spectra of EA–$CdCl_4$ are reported in the frequency range (50–350) cm^{-1} by various groups,[21,23,40] vibrational spectra for internal modes for organic ion have not been reported. R. Kind *et al.* have proposed a model of structural transition in $(CH_3NH_3)_2CdCl_4$, where phase transitions are described in terms of dynamic disorder of organic cations between four potential wells.[15] The change in the orientation order of organic ions with temperature leads to structural transitions. This mandates a study of the internal vibrations of organic ions. In the present study, we have attempted to analyse the temperature dependent Raman spectra for EA–$CdCl_4$ in the frequency range 150–4500 cm^{-1} to understand the dynamics of structural phase transition. Fig. 7 shows the spectra collected at room temperature, 220 K and 77 K which highlight significant changes in the modes observed at both temperatures. All the Raman active modes in the compound are assigned based on the calculation (using the Gaussian software) presented in Table 1 and are well supported by the literature.[21,41] The modes in various regions are divided into the following frequency classes: (i) Cd–Cl bending and stretching modes 150–300 cm^{-1}, (ii) C–N and C–H stretching modes 1000–1050 cm^{-1}, (iii) symmetric and antisymmetric NHH bending 1350–1800 cm^{-1} and (iv) symmetric and antisymmetric NHH stretching 3000–3200 cm^{-1}. In addition, we also observed several modes arising due to N–H···Cl hydrogen bonds, torsional motion of molecular subunits and combination modes and overtone of C–N and C–H vibrations.

Table 1 Calculated vibrational wave-numbers, observed Raman band positions and assignment for $(C_2H_5NH_3)_2CdCl_4$

Calculated	Experimental	Mode assignment
191	176	δ(Cd–Cl)
206	216	ν(Cd–Cl)
268	275	$\tau(NH_3)$
384	409	$\rho(NH_3)$
805	798	$\rho(NH_3)$
865	870	ν(C–N)
963	971	$\rho(NH_3)$
1005	1047	δ(C–C–N) bend
1177	1186	$\delta_s(NH_3)$
1212	1216	$\delta_s(NH_3)$, $\delta_s(NH_3)$
1314	1333	δNH_3, $\delta(CH_2)$
1370	1375	$\delta(CH_2)$ (umbrella reformation)
1461	1465	$\delta(CH_2)$ (scissoring), $\delta_a(CH_3)$
1631	1613	δ(N–H) (bend), $\delta(NH_3)$
2945	2891	$\nu_s(CH_3)$
2982	2939	ν(N–H), $\nu_s(CH_2)$
2989	2972	ν(N–H), $\nu_s(CH_2)$
3003	2990	ν(N–H)
3050	3039	ν(N–H)
3130	3070	$\nu(N–H_2)$
3169	3098	ν_a(N–H)
3264	3158	ν_a(N–H)

ν stretching; δ deformation; ρ rocking; τ torsion.

Near the phase transition temperatures, significant spectral changes are observed. The transitions are in agreement with the transition temperatures reported in single crystal X-ray diffraction study[14] and dielectric measurements reported in the present work. We used the temperature evolution of vibrational frequencies and full width at half maximum (FWHM) related to vibrations/bending modes of various molecular subunits to explain the dynamics driving these phase transitions. At room temperature, EA–$CdCl_4$ is in the *Bmab* orthorhombic phase and the ethyl-ammonium ions are disordered with two symmetrically equivalent orientations as shown by the X-Ray diffraction studies.[14] Below the phase transition (216 K) only one orientation remains and the system transforms to the *Pbca* space group. The spectral features below 300 cm^{-1} matches well with earlier investigations. The frequency of internal vibrations of the $C_2H_5NH_3^+$ molecular group generally lies above 300 cm^{-1}, so the molecular groups can be considered rigid with only translational and rotational (libration) degrees of freedom. Three frequencies centred at 122, 170, and 216 are observed in the spectral region below 300 cm^{-1} as shown in

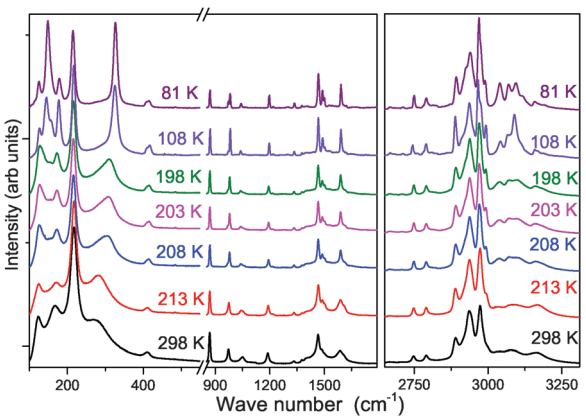

Fig. 7 Raman spectra of $(C_2H_5NH_3)_2CdCl_4$ at 77 K and 300 K in the frequency range (150–4500) cm^{-1}.

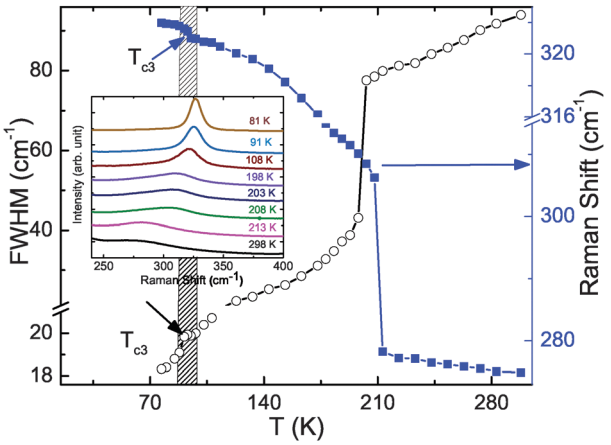

Fig. 8 Temperature evolution of Raman shift and fwhm of the torsional mode of NH_3. Inset shows temperature evolution of the NH_3 torsion mode.

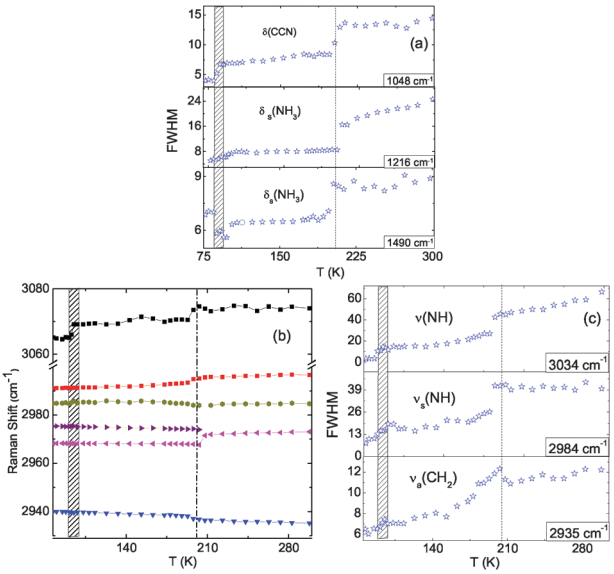

Fig. 9 (a) Temperature evolution of FWHM of various NH_3 deformation modes in the temperature range 77–298 K. (b) Temperature evolution of Raman shift of symmetric and antisymmetric stretching modes of N–H and C–H bonds $(C_2H_5NH_3)_2CdCl_4$. (c) Temperature evolution of FWHM of corresponding vibrational modes in the temperature range 77–298 K.

ESI† (Fig. S1). One more mode is observed at 275 cm^{-1}, which is shown in Fig. 8.

The peak close to 120 cm^{-1} is assigned to the translatory and rotatory modes of the ethyl ammonium group, while the one at 216 cm^{-1} is consequent to symmetrical stretching of the Cd–Cl octahedron due to vibrations of Cd and Cl atoms at axial positions.[21] The frequency mode observed at 170 cm^{-1} arises from displacements of axial and equatorial chlorine atoms which cause Cd–Cl bending.[21] A broad feature is observed at 275 cm^{-1} which is assigned to the internal torsional motion of NH_3 in the organic group.[40] It is worth noting that in the isolated $CH_3NH_3^+$ group, NH_3 torsion motion is neither Raman nor IR active. So even in $C_2H_5NH_3^+$, it is supposed to be inactive. The presence of torsional mode is attributed to the intramolecular interactions of NH_3 with chlorine atoms through N–H···Cl hydrogen bonds. This band shifts to higher frequency below T_{c2}, as shown in Fig. 8. Upon cooling from room temperature to 77 K, we observe abrupt changes for frequencies 168 and 275 cm^{-1} near T_{c2}, while minute changes are seen in the vicinity of T_{c3} = 114 K. The abrupt shift to higher frequency in the torsional mode of NH_3 upon cooling is consistent with hydrogen bond strengthening at low temperature, due to ordering of the organic ion chain.

In the range 500–1750 cm^{-1} several deformation and C–N, C–H stretching modes are observed, as seen in Table 1. The temperature evolution of these modes is shown in ESI,† Fig. S2 and S3. Many of these modes undergo marked changes across T_{c2}, while negligible or no change is observed across T_{c3}. FWHM of few deformation modes of NH_3 show small changes across T_{c3} as shown in Fig. 9(a).

The stretching modes of the ammonium end of the alkyl ammonium ion are presented in Fig. 9(b) and (c). The stretching modes of X–H (X = O, N...) seen in the high frequency region above 2000 cm^{-1} do not interact with other vibrations except X–H stretches. X–H bonds can easily form hydrogen bonding X–H···, which drastically lowers the stretching frequency but are identified from broadening and intensification of bands/modes. Although the hydrogen bond has a weak interaction, it produces significant changes in the vibrational spectra. In EA–$CdCl_4$, hydrogen bonds with chlorine (Cl), resulting in lowering of N–H and C–H stretching modes. C–H symmetric and antisymmetric stretching modes typically occur in the range 2800 to 3000 cm^{-1}. One symmetric (2889 cm^{-1}) and two antisymmetric stretching modes at 2972 and 2982 cm^{-1} are seen in this range, for the $-CH_3$ group. The asymmetric peak at 2972 cm^{-1} softens with temperature and abruptly shifts to 2968 cm^{-1} at T_{c2} and splits to give one more mode at 2974 cm^{-1}. The CH_2 group associated with N, also gives rise to a C–H antisymmetric stretching mode at 2923 cm^{-1}, which splits to give rise to another peak while approaching T_{c3}. Due to vibrational coupling between identical C–H vibrational modes sharing the same C atom, 3 additional frequencies are evident: one symmetric and 2 anti-symmetric. The former occurs at low frequency, while the antisymmetric mode occurs at higher frequency. There is no coupling between C–H modes belonging to different C atoms. Similarly, N–H symmetric and antisymmetric stretching modes are observed in the range 2900 to 3200 cm^{-1}. N–H stretching generally correspond to 3400 cm^{-1} but the frequency reduces sharply in the case of hydrogen bonding. In $(C_2H_5NH_3)_2CdCl_4$, N–H forms a hydrogen bond with the Cl atom of the Cd–Cl octahedron which lowers the frequency of N–H stretching modes resulting in modes at 2990 cm^{-1} (symmetric); 3073 and 3098 cm^{-1} (antisymmetric). Other modes are seen at 3035 and 3185 cm^{-1} due to coupling between identical N–H stretching. All modes in this region soften with a decrease in temperature and anomalies are seen at both T_{c2} and T_{c3}.

Raman studies show significant changes in the temperature dependence of the wavenumber and FWHM of various vibrational modes in the proximity of the structural transitions observed below room temperature. The temperature dependence of internal modes

and its FWHM of organic cations consolidates their (reorientation order) role in structural modifications. The observed results are consistent with the theoretical predications for $(CH_3NH_3)_2CdCl_4$. From the structural data available, it is known that at room temperature, the system is disordered and the C–C bond is constrained to lie on a mirror plane yielding two equivalent positions for the organic chain. Hence, the symmetry equivalent chains influence the Cd–Cl octahedron *via* hydrogen bonding leading to an anomaly in the bending mode for the octahedron across T_{c2}. The number of symmetrically equivalent sites reduces resulting in structural transition at T_{c2} which is reflected in the vibrational modes associated with both Cd–Cl octahedron and external and internal vibrations of the organic chain. The monoclinic transition cannot be explained in terms of the order–disorder model. Further it can be explained in terms of non-linear coupling of organic chain motion with the Cd–Cl octahedron. Since, the Cd–Cl octahedron is weakly coupled with the organic chain through hydrogen bonding, the changes in vibrational spectra at T_{c3} are not as prominent as that at T_{c2}. Very few modes associated with C–N and N–H stretching modes show small variation across T_{c3}. Despite lack of single crystal data to confirm the existence of a monoclinic phase at low temperature, theoretical calculations and Raman studies on $(CH_3NH_3)_2CdCl_4$ predict a monoclinic phase with space group $P2_1/b$. $(C_2H_5NH_3)_2CdCl_4$ also belongs to the same family of compounds and a similar monoclinic structure has been predicted. It is worth noting that the $P2_1/b$ space group is a maximal subgroup of the *Pbca* space group and does not satisfy the Landau condition[42] for a second-order transition according to the Geick and Strobel criterion.[43] This implies the presence of first order transition which has been seen in the heating and cooling cycles of dielectric measurements. However, the observed Raman behaviour of a few NH_3 vibration modes across T_{c3} points out to a first order-like transition, instead of strongly first order nature and occurs over a broad range of temperature. On the basis of linewidth as a function of temperature, it can be asserted that this transition is related to torsion and libration motions of organic groups and is associated with a small distortion of the lattice. The transition is displacive in nature, rather than an order–disorder transition and is therefore very weak in nature, manifested only in few Raman modes belonging to the motion of organic groups.

On the basis of dielectric and Raman studies, we postulate 4 phases of $(C_2H_5NH_3)_2CdCl_4$ evolving with temperature. The system consolidates into a tetragonal $I4/mmm$ phase at high temperature. As the material is cooled, it undergoes structural transition to the orthorhombic *Bmab* phase, which later transforms to the *Pcab* phase at about 214 K. Further an addition structural transition is observed below 110 K where the system changes to monoclinic symmetry.

4 Conclusion

The dynamics of phase transitions in $(C_2H_5NH_3)_2CdCl_4$ are understood by dielectric and Raman studies. The anomalies observed in vibrational frequencies and fwhm at transition temperature are attributed to phase transitions. Dielectric measurements regard these anomalies in the perspective of three transition temperatures. The phase transitions are driven by the ordering of the $(C_2H_5NH_3)^+$ ion. Internal vibrations of N–H and C–N stretching modes and their FWHM provide additional insight into the ordering mechanism for low temperature transitions. The high temperature dielectric response describes relaxation behaviour and is believed to be considerably different from the ideal Debye type relaxation. The dielectric constant increases with temperature while the relaxation time decreases for the high temperature phase. The observed decrease in relaxation time can be correlated with weakening of H-bonds as the temperature increases. The determined relaxation time is characteristic of the combined reorientation of ethylammonium groups. Raman and dielectric studies confirm the existence of all 4 phases in $(C_2H_5NH_3)_2CdCl_4$.

Acknowledgements

Ruchika Yadav and Partha P. Kundu wish to acknowledge Council for Scientific and Industrial Research, India, for fellowship. Thanks are due to Department of Science and Technology, India, for financial support through project grant.

References

1 A. K. Cheetham and C. N. R. Rao, *Science*, 2007, **318**, 58–59.
2 A. H. Arkenbout, T. Uemura, J. Takeya and T. T. M. Palstra, *Appl. Phys. Lett.*, 2009, **95**, 173104.
3 S. Kitagawa, R. Kitaura and S.-i. Noro, *Angew. Chem., Int. Ed.*, 2004, **43**, 2334–2375.
4 C. N. R. Rao, A. K. Cheetham and A. Thirumurugan, *J. Phys.: Condens. Matter*, 2008, **20**, 083202.
5 O. M. Yaghi, G. Li and H. Li, *Nature*, 1995, **378**, 703–706.
6 A. K. Cheetham, C. N. R. Rao and R. K. Feller, *Chem. Commun.*, 2006, 4780.
7 D. B. Mitzi, *J. Chem. Soc., Dalton Trans.*, 2001, 1–12.
8 D.-f. Weng, Z.-m. Wang and S. Gao, *Chem. Soc. Rev.*, 2011, **40**, 3157–3181.
9 M. Kurmoo, *Chem. Soc. Rev.*, 2009, **38**, 1353–1379.
10 W. Zhang and R.-g. Xiong, *Chem. Rev.*, 2012, **112**, 1163–1195.
11 P. Jain, V. Ramachandran, R. J. Clark, H. D. Zhou, B. H. Toby, N. S. Dalal, H. W. Kroto and A. K. Cheetham, *J. Am. Chem. Soc.*, 2009, **131**, 13625–13627.
12 M. Sánchez-Andújar, S. Presedo, S. Yáñez Vilar, S. Castro-Garcá, J. Shamir and M. A. Señarís Rodríguez, *Inorg. Chem.*, 2010, **49**, 1510–1516.
13 G.-c. Xu, W. Zhang, X.-M. Ma, Y.-h. Chen, L. Zhang, H.-l. Cai, Z.-m. Wang, R.-g. Xiong and S. Gao, *J. Am. Chem. Soc.*, 2011, **133**, 14948–14951.
14 G. Chapuis, *Phys. Status Solidi*, 1977, **43**, 203–212.
15 R. Kind, R. Blinc and B. Zeks, *Phys. Rev. B: Condens. Matter Mater. Phys.*, 1979, **19**, 3743–3754.

16 J. Steadman and R. Willett, *Inorg. Chim. Acta*, 1970, **4**, 367–371.
17 B. Kundys, A. Lappas, M. Viret, V. Kapustianyk, V. Rudyk, S. Semak, C. Simon and I. Bakaimi, *Phys. Rev. B: Condens. Matter Mater. Phys.*, 2010, **81**, 224434.
18 Y. Takehisa, *J. Phys. Soc. Jpn.*, 1989, **58**, 2276.
19 K. Ohwada, K. Ishii, T. Inami, Y. Murakami, T. Shobu, H. Ohsumi, N. Ikeda and Y. Ohishi, *Phys. Rev. B: Condens. Matter Mater. Phys.*, 2005, **72**, 014123.
20 V. Kapustianyk, V. Rudyk and M. Partyka, *Phys. Status Solidi*, 2007, **244**, 2151–2158.
21 H. Hagemann and H. Bill, *J. Phys. C: Solid State Phys.*, 1985, **18**, 6441–6456.
22 R. Kind, *Ferroelectrics*, 1980, **24**, 81–88.
23 H. Hagemann and H. Bill, *Chem. Phys. Lett.*, 1982, **87**, 45–49.
24 M. Couzi, A. Daoud and R. Perret, *Phys. Status Solidi*, 1977, **41**, 271–282.
25 G. V. P. Kumar and C. Narayana, *Curr. Sci.*, 2007, **93**, 778–791.
26 M. Frisch, G. Trucks, H. Schlegel, G. Scuseria, M. Robb, J. Cheesemann, V. Zakrzewski, J. Montgomery Jr, R. Stratmann and J. Burant, *et al.*, GAUSSIAN software, 2009.
27 A. D. Becke, *J. Chem. Phys.*, 1993, **98**, 5648.
28 C. Lee, W. Yang and R. G. Parr, *Phys. Rev. B: Condens. Matter Mater. Phys.*, 1988, **37**, 785, DOI: 10.1103/PhysRevB.37.785.
29 P. J. Hay and W. R. Wadt, *J. Chem. Phys.*, 1985, **82**, 270.
30 R. D. Johnson III, Johnson III http://srdata.nist.gov/cccbdb, 2005.
31 A. Levstik and C. Filipic, *Phys. Status Solidi*, 1980, **58**, K165–K166.
32 Y. Korchak, V. Kapustianik, R. Tchukvinskyi, Z. Czapla, S. Dacko and V. Bazhan, *Phys. Status Solidi*, 2001, **228**, 777–784.
33 J. Han, S. Nishihara, K. Inoue and M. Kurmoo, *Inorg. Chem.*, 2014, **53**, 2068–2075.
34 D. Zhou, W.-B. Li, L.-X. Pang, Z.-X. Yue, G.-S. Pang and X. Yao, *RSC Adv.*, 2015, **5**, 19255–19258.
35 B. Pato-Doldán, M. Sánchez-Andújar, L. Gómez-Aguirre, S. Yáñez-Vilar, J. López-Beceiro, C. Gracia-Fernández, A. Haghighirad, F. Ritter, S. Castro-Garcá and M. Señarís-Rodríguez, *Phys. Chem. Chem. Phys.*, 2012, **14**, 8498–8501.
36 T. Besara, P. Jain, N. S. Dalal, P. L. Kuhns, A. P. Reyes, H. W. Kroto and A. K. Cheetham, *Proc. Natl. Acad. Sci. U. S. A.*, 2011, **108**, 6828–6832.
37 V. B. Kapustianik, H. Kabelka, H. Warhanek and A. Fuith, *Phys. Status Solidi*, 1996, **155**, 95–113.
38 V. Kapustianik, I. Polovinko, Y. Korchak, S. Sveleba, R. Tchukvinskyi and S. Kaluza, *Phys. Status Solidi*, 1997, **161**, 515–521.
39 I. R. Jahn, K. Schwab, K. Knorr and K. Holocher, *J. Phys.: Condens. Matter*, 1994, **6**, 10839–10853.
40 R. Mokhlisse, *J. Chem. Phys.*, 1982, **77**, 1138.
41 D. W. Mayo, F. A. Miller and R. W. Hannah, *Course Notes on the Interpretation of Infrared and Raman Spectra*, John Wiley & Sons, Inc., Hoboken, NJ, USA, 2004.
42 A. Bruce and R. A. Cowley, *Structural phase transitions*, Taylor and Francis, 1981, vol. 29.
43 R. Geick and K. Strobel, *J. Phys. C: Solid State Phys.*, 1977, **10**, 4221.

